

Four-wave mixing in slow light engineered silicon photonic crystal waveguides

C. Monat,^{1,*} M. Ebnali-Heidari,² C. Grillet,¹ B. Corcoran,¹ B. J. Eggleton,¹ T. P. White,³ L. O'Faolain,³ J. Li,³ and T. F. Krauss³

¹Centre for Ultrahigh-bandwidth Devices for Optical Systems (CUDOS), Institute for Photonics and Optical Sciences (IPOS), School of Physics, University of Sydney, NSW 2006, Australia

²Faculty of Engineering, University of Shahrekord, Shahrekord, Iran

³School of Physics and Astronomy, University of St. Andrews, St. Andrews, Fife, KY16 9SS, UK

*monat@physics.usyd.edu.au

Abstract: We experimentally investigate four-wave mixing (FWM) in short (80 μm) dispersion-engineered slow light silicon photonic crystal waveguides. The pump, probe and idler signals all lie in a 14 nm wide low dispersion region with a near-constant group velocity of $c/30$. We measure an instantaneous conversion efficiency of up to -9dB between the idler and the continuous-wave probe, with 1W peak pump power and 6nm pump-probe detuning. This conversion efficiency is found to be considerably higher ($>10\times$) than that of a Si nanowire with a group velocity ten times larger. In addition, we estimate the FWM bandwidth to be at least that of the flat band slow light window. These results, supported by numerical simulations, emphasize the importance of engineering the dispersion of PhC waveguides to exploit the slow light enhancement of FWM efficiency, even for short device lengths.

©2010 Optical Society of America

OCIS codes: (190.4380) Nonlinear optics; four-wave mixing; (130.5296) Photonic crystal waveguides; (260.2030) Dispersion.

References and links

1. T. F. Krauss, "Why do we need slow light?" *Nat. Photonics* **2**(8), 448–450 (2008).
2. T. Baba, "Slow light in photonic crystals," *Nat. Photonics* **2**(8), 465–473 (2008).
3. M. Soljačić, S. G. Johnson, S. H. Fan, M. Ibanescu, E. Ippen, and J. D. Joannopoulos, "Photonic-crystal slow-light enhancement of nonlinear phase sensitivity," *J. Opt. Soc. Am. B* **19**(9), 2052–2059 (2002).
4. N. A. R. Bhat, and J. E. Sipe, "Optical pulse propagation in nonlinear photonic crystals," *Phys. Rev. E Stat. Nonlin. Soft Matter Phys.* **64**(5 Pt 2), 056604–056604 (2001).
5. C. Monat, B. Corcoran, M. Ebnali-Heidari, C. Grillet, B. J. Eggleton, T. P. White, L. O'Faolain, and T. F. Krauss, "Slow light enhancement of nonlinear effects in silicon engineered photonic crystal waveguides," *Opt. Express* **17**(4), 2944–2953 (2009).
6. K. Inoue, H. Oda, N. Ikeda, and K. Asakawa, "Enhanced third-order nonlinear effects in slow-light photonic-crystal slab waveguides of line-defect," *Opt. Express* **17**(9), 7206–7216 (2009).
7. A. Baron, A. Ryasnyanskiy, N. Dubreuil, P. Delaye, Q. Vy Tran, S. Combrié, A. de Rossi, R. Frey, and G. Roosen, "Light localization induced enhancement of third order nonlinearities in a GaAs photonic crystal waveguide," *Opt. Express* **17**(2), 552–557 (2009).
8. Y. Hamachi, S. Kubo, and T. Baba, "Slow light with low dispersion and nonlinear enhancement in a lattice-shifted photonic crystal waveguide," *Opt. Lett.* **34**(7), 1072–1074 (2009).
9. C. Husko, S. Combrié, Q. V. Tran, F. Raineri, C. W. Wong, and A. De Rossi, "Non-trivial scaling of self-phase modulation and three-photon absorption in III-V photonic crystal waveguides," *Opt. Express* **17**(25), 22442–22451 (2009).
10. B. Corcoran, C. Monat, C. Grillet, D. J. Moss, B. J. Eggleton, T. P. White, L. O'Faolain, and T. F. Krauss, "Green light emission in silicon through slow-light enhanced third-harmonic generation in photonic crystal waveguides," *Nat. Photonics* **3**(4), 206–210 (2009).
11. C. Monat, C. Grillet, B. Corcoran, D. J. Moss, B. J. Eggleton, T. P. White, and T. F. Krauss, "Investigation of phase matching for third-harmonic generation in silicon slow light photonic crystal waveguides using Fourier optics," *Opt. Express* **18**(7), 6831–6840 (2010).
12. C. Monat, B. Corcoran, D. Pudo, M. Ebnali-Heidari, C. Grillet, M. D. Pelusi, D. J. Moss, B. J. Eggleton, T. P. White, L. O'Faolain, and T. F. Krauss, "Slow light enhanced nonlinear optics in silicon photonic crystal waveguides," *IEEE J. Sel. Top. Quantum Electron.* **16**, 344–356 (2010).

13. D. Pudo, B. Corcoran, C. Monat, M. Pelusi, D. Moss, B. J. Eggleton, T. P. White, L. O'Faolain, and T. F. Krauss, "Investigation of slow light enhanced nonlinear transmission for all-optical regeneration in silicon photonic crystal waveguides at 10 Gbit/s," *Photonics Nanostruct. Fundam. Appl.* **8**(2), 67–71 (2010).
14. B. Corcoran, C. Monat, D. Pudo, B. J. Eggleton, T. F. Krauss, D. J. Moss, L. O'Faolain, M. Pelusi, and T. P. White, "Nonlinear loss dynamics in a silicon slow-light photonic crystal waveguide," *Opt. Lett.* **35**(7), 1073–1075 (2010).
15. J. Li, T. P. White, L. O'Faolain, A. Gomez-Iglesias, and T. F. Krauss, "Systematic design of flat band slow light in photonic crystal waveguides," *Opt. Express* **16**(9), 6227–6232 (2008).
16. L. H. Frandsen, A. V. Lavrinenko, J. Fage-Pedersen, and P. I. Borel, "Photonic crystal waveguides with semi-slow light and tailored dispersion properties," *Opt. Express* **14**(20), 9444–9450 (2006).
17. S. Kubo, D. Mori, and T. Baba, "Low-group-velocity and low-dispersion slow light in photonic crystal waveguides," *Opt. Lett.* **32**(20), 2981–2983 (2007).
18. M. Ebnali-Heidari, C. Grillet, C. Monat, and B. J. Eggleton, "Dispersion engineering of slow light photonic crystal waveguides using microfluidic infiltration," *Opt. Express* **17**(3), 1628–1635 (2009).
19. T. F. Krauss, L. O'Faolain, S. Schulz, D. M. Beggs, F. Morichetti, A. Canciamilla, A. Melloni, P. Lalanne, A. Samarelli, M. Sorel, and R. M. De La Rue, "Understanding the rich physics of light propagation in slow photonic crystal waveguides," *Proc. Soc. Photo Opt. Instrum. Eng.* **7612**, 76120L (2010) (SPIE).
20. A. Melloni, A. Canciamilla, C. Ferrari, F. Morichetti, L. O'Faolain, T. F. Krauss, R. De La Rue, A. Samarelli, and M. Sorel, "Tunable delay lines in silicon photonics: coupled resonators and photonic crystals, a comparison," *IEEE Photonics J.* **2**(2), 181–194 (2010).
21. B. Corcoran, C. Monat, M. Pelusi, C. Grillet, T. P. White, L. O'Faolain, T. F. Krauss, B. J. Eggleton, and D. J. Moss, "Optical signal processing on a silicon chip at 640Gb/s using slow-light," *Opt. Express* **18**(8), 7770–7781 (2010).
22. M. A. Foster, A. C. Turner, J. E. Sharping, B. S. Schmidt, M. Lipson, and A. L. Gaeta, "Broad-band optical parametric gain on a silicon photonic chip," *Nature* **441**(7096), 960–963 (2006).
23. M. R. E. Lamont, B. T. Kuhlmeier, and C. M. de Sterke, "Multi-order dispersion engineering for optimal four-wave mixing," *Opt. Express* **16**(10), 7551–7563 (2008).
24. M. R. Lamont, B. Luther-Davies, D.-Y. Choi, S. Madden, X. Gai, and B. J. Eggleton, "Net-gain from a parametric amplifier on a chalcogenide optical chip," *Opt. Express* **16**(25), 20374–20381 (2008).
25. B. G. Lee, A. Biberman, A. C. Turner-Foster, M. A. Foster, M. Lipson, A. L. Gaeta, and K. Bergman, "Demonstration of Broadband Wavelength Conversion at 40 Gb/s in Silicon Waveguides," *IEEE Photon. Technol. Lett.* **21**(3), 182–184 (2009).
26. M. Ebnali-Heidari, C. Monat, C. Grillet, and M. K. Moravvej-Farshi, "A proposal for enhancing four-wave mixing in slow light engineered photonic crystal waveguides and its application to optical regeneration," *Opt. Express* **17**(20), 18340–18353 (2009).
27. V. Eckhouse, I. Cestier, G. Eisenstein, S. Combr e, P. Colman, A. De Rossi, M. Santagiustina, C. G. Someda, and G. Vadal , "Highly efficient four wave mixing in GaInP photonic crystal waveguides," *Opt. Lett.* **35**(9), 1440–1442 (2010).
28. K. Suzuki, Y. Hamachi, and T. Baba, "Fabrication and characterization of chalcogenide glass photonic crystal waveguides," *Opt. Express* **17**(25), 22393–22400 (2009).
29. J. F. McMillan, M. Yu, D. L. Kwong, and C. W. Wong, "Observation of four-wave mixing in slow-light silicon photonic crystal waveguides," *Opt. Express* **18**(15), 15484–15497 (2010).
30. G. P. Agrawal, *Nonlinear fiber optics*, 2nd Edition (Academic Press, San Diego 1995).
31. L. Jia, M. Geng, L. Zhang, L. Yang, P. Chen, Y. Liu, Q. Fang, and M. Yu, "Effects of waveguide length and pump power on the efficiency of wavelength conversion in silicon nanowire waveguides," *Opt. Lett.* **34**(22), 3502–3504 (2009).
32. M. A. Foster, A. C. Turner, R. Salem, M. Lipson, and A. L. Gaeta, "Broad-band continuous-wave parametric wavelength conversion in silicon nanowaveguides," *Opt. Express* **15**(20), 12949–12958 (2007).
33. H. S. Rong, Y. H. Kuo, A. S. Liu, M. Paniccia, and O. Cohen, "High efficiency wavelength conversion of 10 Gb/s data in silicon waveguides," *Opt. Express* **14**(3), 1182–1188 (2006).
34. K. Yamada, H. Fukuda, T. Tsuchizawa, T. Watanabe, T. Shoji, and S. Itabashi, "All-optical efficient wavelength conversion using silicon photonic wire waveguide," *IEEE Photon. Technol. Lett.* **18**(9), 1046–1048 (2006).
35. R. Salem, M. A. Foster, A. C. Turner, D. F. Geraghty, M. Lipson, and A. L. Gaeta, "Signal regeneration using low-power four-wave mixing on silicon chip," *Nat. Photonics* **2**(1), 35–38 (2008).
36. W. Mathlouthi, H. Rong, and M. Paniccia, "Characterization of efficient wavelength conversion by four-wave mixing in sub-micron silicon waveguides," *Opt. Express* **16**(21), 16735–16745 (2008).
37. Y. H. Kuo, H. S. Rong, V. Sih, S. B. Xu, M. Paniccia, and O. Cohen, "Demonstration of wavelength conversion at 40 Gb/s data rate in silicon waveguides," *Opt. Express* **14**(24), 11721–11726 (2006).
38. M. W. Lee, C. Grillet, C. G. Poulton, C. Monat, C. L. C. Smith, E. M gi, D. Freeman, S. Madden, B. Luther-Davies, and B. J. Eggleton, "Characterizing photonic crystal waveguides with an expanded k-space evanescent coupling technique," *Opt. Express* **16**(18), 13800–13808 (2008).
39. S. Combr e, Q. V. Tran, A. De Rossi, C. Husko, and P. Colman, "High quality GaInP nonlinear photonic crystals with minimized nonlinear absorption," *Appl. Phys. Lett.* **95**(22), 221108 (2009).

1. Introduction

Propagation of slow light in planar photonic crystal (PhC) waveguides has recently attracted significant attention for its potential to increase the efficiency of nonlinear optical phenomena per unit length [1–4]. The expected reduction in both the required path length and the power consumption of the associated devices makes this platform promising for on-chip all-optical signal processing. Several groups have recently demonstrated that nonlinear effects associated with self-phase modulation [5–8], two-photon [5–8] and three-photon absorption [9], and third-harmonic generation [10,11] were strongly enhanced by slow light in PhC waveguides made of III-V semiconductors [6,7,9] and silicon [5,8,10–12]. Although the simultaneous slow light enhancement of nonlinear losses can be interesting for specific applications such as optical limiting [13,14], it generally restricts, along with linear losses, the effective path length and power regime for which slow light devices can be advantageously used [12]. The most significant benefit of using slow light PhC waveguides in silicon therefore lies in the realisation of short nonlinear devices ($<100\mu\text{m}$), at least with the present technology. In addition, the possibility of engineering the high-order dispersion of PhC waveguides to create slow light features with wide bandwidth (or flat-band slow light) [15–18] and relatively low linear loss [19,20] has enabled the demonstration of all-optical signal processing at bit rates close to the Terabit/s regime [21].

Four-wave mixing (FWM) should similarly benefit from slow light in PhC waveguides because it relies on the same $\chi^{(3)}$ nonlinear response of the medium as the processes mentioned above. The possibility of engineering the high-order dispersion of these waveguides makes them even more compelling for such applications, because the efficiency and bandwidth of FWM processes can be critically increased by optimizing the dispersion, as shown in rib waveguides and nanowires [22–25]. The 2D geometry of the PhC waveguide expands the design flexibility for engineering the dispersion while still providing high nonlinear γ parameters, in contrast to standard waveguides, where the cross-section area and the dispersion characteristics are linked. In this context, we have theoretically studied how slow light dispersion engineered PhC waveguides can promote both the efficiency and bandwidth of FWM in a short device [26]. Several groups have recently reported FWM in PhC waveguides made of III-V [27], chalcogenide [28] and silicon [29]. However, these demonstrations have been restricted to the use of standard W1 PhC waveguides, where the issue of loss and high-order dispersion at the band-edge makes it difficult to exploit slow light modes efficiently, and strongly restricts the bandwidth of FWM conversion to typically less than 1 or 2nm. This severely limits the practical application of FWM in these structures.

Here, we experimentally demonstrate FWM in a short ($80\mu\text{m}$) silicon slow light ($c/30$) dispersion engineered PhC waveguide through launching a low repetition rate pulsed pump and a continuous-wave (cw) probe. We extract an instantaneous conversion efficiency between the idler and the probe of -9dB , which compares favourably to previous demonstrations in W1 PhC waveguides [27,29] and also to the performance of centimetre long silicon nanowires [25]. We directly demonstrate that slow light propagation in PhC waveguides increases the FWM efficiency by comparing the results to those of a Si nanowire with a ten-times higher group velocity. The measured enhancement ($>10\times$) is limited by the contribution from the access waveguides and occurs despite the increase of linear and nonlinear loss in the slow light PhC waveguide, which manifests as a strong saturation of both the transmission and the conversion efficiency above $\sim 1\text{W}$ peak pump power. The bandwidth of the FWM conversion is measured to be $>14\text{nm}$, i.e. similar to the bandwidth of the low dispersion slow light region of the PhC waveguide. Simulations using the split-step Fourier method (SSFM) support the measurements.

2. Description of the device and the experimental setup

The PhC waveguide is similar to ref [5] and consists of a modified W1 waveguide, made in a 220nm thick suspended silicon membrane [see Fig. 1(b)]. The geometry of the PhC waveguide is engineered by shifting the first two rows of holes either side of the waveguide in

the lateral direction [15] to produce a flat band slow light region where the group velocity v_g is low ($v_g \sim c/n_g \sim c/30$) and constant to within $\pm 10\%$ over a 14nm window [see Fig. 1(c)]. The slow-down factor $S = n_g/n$ of this waveguide is thus a bit smaller than 10. The high-order dispersion parameters $\beta_2 = 1.3 \times 10^{-21} \text{ s}^2/\text{m}$ and $\beta_4 = -6 \times 10^{-46} \text{ s}^4/\text{m}$ at the centre of the slow light window ($\sim 1559\text{nm}$) are estimated from 3D plane wave band structure calculations that have been matched to the experimental dispersion of Fig. 1(c). The 80 μm -long PhC waveguide is connected on both sides to a 0.4 mm long, 3 μm wide waveguide tapered in width over 200 μm to improve light insertion. The same chip includes an 80 μm long silicon nanowire accessed by similar tapered waveguides. Despite its smaller cross-section area (700nm \times 220nm \sim 0.15 μm^2) than the PhC waveguide mode, the nanowire provides a one order of magnitude faster reference waveguide ($n_g \sim 4$) to be directly compared with the PhC waveguide. From the cross-section mode area ($A_{\text{eff}} \sim 0.5\mu\text{m}^2$) and the nonlinear index n_2 ($= 5.10^{-18} \text{ m}^2/\text{W}$) of silicon, we estimate the effective nonlinear parameter $\gamma \sim [2\pi n_2 / (\lambda \cdot A_{\text{eff}})] S^2$ to be $\sim 2900/\text{W}/\text{m}$ for the slow light PhC waveguide [12]. This is more than one order of magnitude larger than for the reference nanowire ($\gamma \sim 170/\text{W}/\text{m}$) due to the slow light enhancement of γ but this is less than a factor S^2 larger due to the smaller A_{eff} of the nanowire. We consider the nonlinear contribution from the wide access ridge to be negligible due to its low γL product ($30 \times 8.10^{-4} \sim 0.024/\text{W}$) as compared to that of the slow light PhC waveguide ($\gamma L \sim 0.23/\text{W}$). However, as discussed in section 3.3, this contribution cannot be neglected for the nanowire, for which γL is $\sim 0.014/\text{W}$.

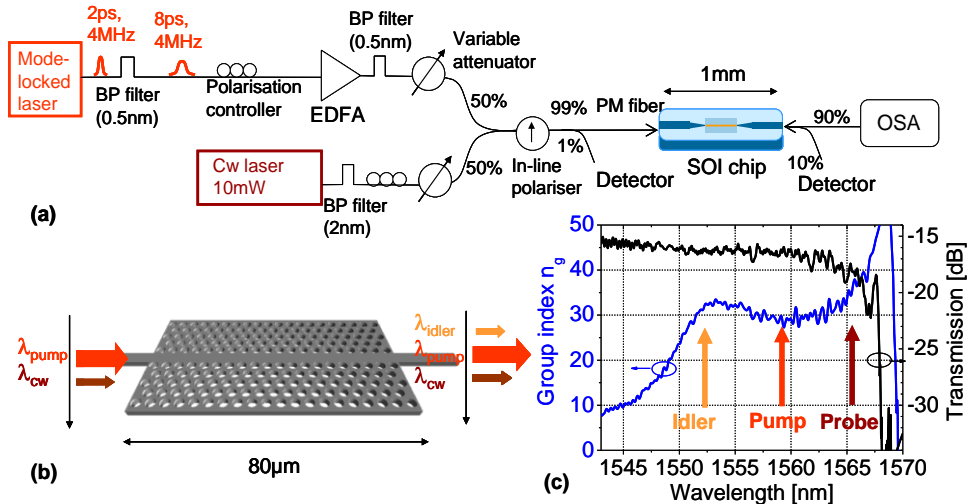


Fig. 1. (a-b) Schematic of the set-up associated with the partially degenerate FWM configuration investigated here along with the probed planar PhC waveguide. (c) Spectral variation of the group index for the dispersion engineered PhC waveguide with the wavelength of the probe, pump and idler highlighted.

We measure FWM in these waveguides using a degenerate pump configuration. The set-up [Fig. 1(a) and 1(b)] mixes a low repetition rate (4MHz) train of 8 picosecond pulses (pump) generated by a filtered and amplified mode-locked fiber laser with a cw laser (probe). The output is measured independently with a photodetector and an optical spectrum analyzer (OSA) with a resolution bandwidth of 0.5nm. Both pump and probe signals are tunable around 1550nm and their polarization is controlled so as to excite primarily the TE fundamental mode in the waveguide. The pump and probe peak powers launched at the input of the waveguides through lensed fibers are up to 14W and 2mW, respectively. From the total transmission of $\sim -16\text{dB}$ on Fig. 1(c), we estimate the coupling coefficient to be $\sim 20\%$ and the associated powers coupled into the waveguide to be up to 3W and 0.4mW. Coupled (peak) powers will be quoted in the rest of the paper unless stated otherwise. The input patch cord, in

which the pump and probe signals are mixed before coupling into the chip, has a length L of $\sim 1\text{m}$. We therefore estimate its nonlinear contribution through the associated $\gamma P_{\text{pump}}L$ product to be $\sim 5.10^{-3} \times 14 \times 1 \sim 0.07$ at the maximum pump power P_{pump} of 14W and considering a nonlinear $\gamma \sim 5.10^{-3} / \text{W/m}$ for the silica fiber [30]. This value is one order of magnitude lower than the $\gamma P_{\text{pump}}L$ product associated with the PhC waveguide ($\sim 0.23 \times 3 = 0.69$) at the maximum coupled P_{pump} of 3W , suggesting that the nonlinear contribution from the input patch cord is negligible in the FWM experiment involving the PhC waveguide. However, this may add a residual contribution to FWM when probing the nanowire in section 3.3.

The measurements are compared with SSFM numerical simulations [30] obtained from the approximate 1D effective model described in [26], which numerically solves the nonlinear Schrödinger equation governing the propagation of the slowly varying envelope $A(z,t)$ of the pulse electric field amplitude along the nonlinear waveguide. This includes the effects of free carriers, two-photon absorption, second-, third-, and fourth-order dispersion in addition to the optical Kerr effect and accounts for the slow light enhancement of all these effects [5,26].

3. FWM experimental results

3.1 FWM conversion efficiency between the idler and probe signals

Figure 2(a) displays the output spectra from the slow light PhC waveguide for 1W peak pump power at $\sim 1558.7\text{nm}$ and a cw probe power up to $350\mu\text{W}$ at $\sim 1565.5\text{nm}$. As a result of FWM, an idler signal is observed at a wavelength below that of the pump ($\sim 1552\text{nm}$), corresponding to the pump-probe frequency detuning. This is expected from the energy conservation in the degenerate FWM scheme, where two photons from the pump are converted into one probe photon and one idler photon. The pump wavelength is centred on the flat-band slow light window spanning across $1552\text{--}1566\text{nm}$, in order to maximize the conversion efficiency and the FWM bandwidth, as discussed in [26]. Note that all three signals lie within the flat band slow light window, as depicted on Fig. 1(c).

In the approximation of the undepleted pump (and without nonlinear loss), the conversion efficiency η , i.e. the ratio between the idler power $P_{\text{idler}}(L)$ after a propagation distance L in the waveguide and the probe power $P_{\text{probe}}(0)$ coupled at the entrance of the waveguide can be expressed as [26,30]:

$$\eta(L) \equiv \frac{P_{\text{idler}}(L)}{P_{\text{probe}}(0)} = (\gamma \overline{P_{\text{pump}}}(L))^2 \phi \cdot e^{-\alpha L} \quad (1)$$

with

$$\phi = \left(\frac{\sinh(gL)}{gL} \right)^2. \quad (2)$$

The parametric gain $g = \sqrt{(\gamma \overline{P_{\text{pump}}})^2 - (\Delta k / 2)^2}$ depends on the nonlinear phase shift and the net phase mismatch $\Delta k = \Delta k_L + \Delta k_{NL}$ between the pump, probe and idler waves that includes a linear (Δk_L) and a nonlinear ($\Delta k_{NL} = 2 \gamma \overline{P_{\text{pump}}}$) contribution. The path average pump power $\overline{P_{\text{pump}}}(L) = P_{\text{pump}}(0) \cdot (1 - e^{-\alpha L}) / \alpha L$ is reduced by the propagation loss α , and we assume α to be similar for all signals. The phase factor ϕ either reduces η if $g^2 < 0$ ($\phi < 1$), or increases it if $g^2 \geq 0$ ($\phi \geq 1$). The latter occurs when a negative linear phase mismatch Δk_L balances the nonlinear phase mismatch Δk_{NL} , i.e. as long as $0 > \Delta k_L > -2 \gamma \overline{P_{\text{pump}}}$. Because of this, optimizing the waveguide dispersion is critical to FWM, and we expect the engineered PhC waveguide to provide better performance than W1 dispersive waveguides, as discussed in section 4. Lastly, because $g \leq g_{\text{max}}$ with $g_{\text{max}} = \gamma \overline{P_{\text{pump}}}$, this determines an upper value for ϕ and η in Eqs. (1) and (2).

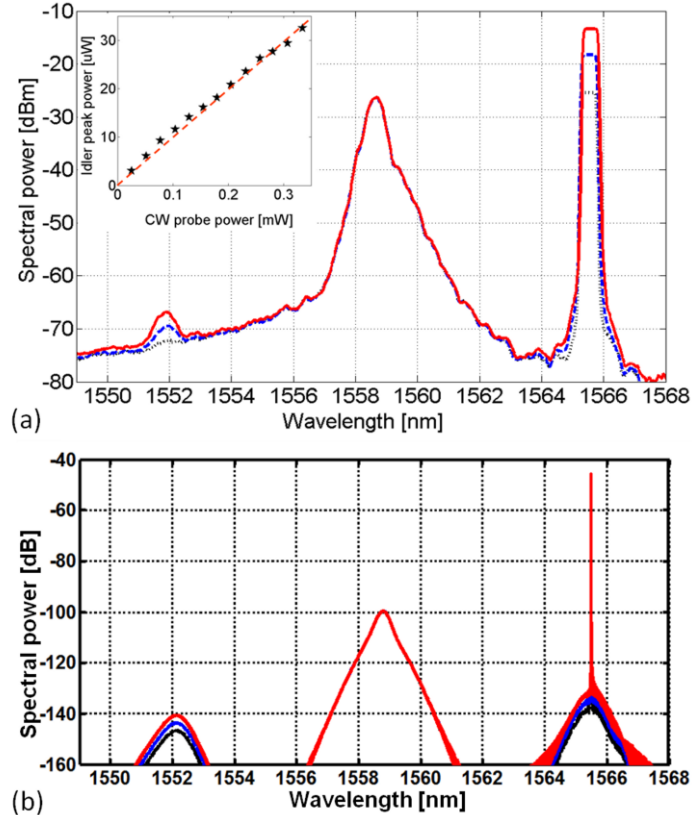


Fig. 2. (a-b) FWM spectra (a) measured and (b) simulated out of the slow light PhC waveguide for a constant 1W coupled peak pump power (at 1558.7nm) and increasing cw probe power from 0.1mW (black dotted line) to 0.4mW (red solid line) at 1565.5nm. Inset: Associated idler peak power at the end of the waveguide versus probe coupled power from (stars) experiments and (dashed red line) simulations.

Compared to previous work, estimating the experimental conversion efficiency is not straightforward here due the different nature of the (pulsed) idler and the (cw) probe signals. In addition, the 0.5nm resolution of the OSA artificially increases the spectral peak power measured for the pulsed signals in Fig. 2(a) with respect to that of the cw probe, whose linewidth is broadened up to ~ 0.5 nm. From the experimental result of Fig. 2(a), we extract, through two different ways, the ratio between the idler peak power ($P_{\text{idler}}(L)$) and the cw probe power ($P_{\text{probe}}(L)$), with both powers measured at the end of the waveguide. The first method consists of calculating the probe and idler average power by integrating the spectral power density (over ~ 1.5 nm) recorded on the OSA around both the idler and probe wavelengths, after subtracting the background power due to the pump (taken from the pump transmission). The ratio of these two average powers is equal to ~ 52 dB. Taking into account the limited time overlap between the (8ps, 4MHz) pulsed pump signal and the cw probe, which is equal to $8 \cdot 10^{-12} / 250 \cdot 10^{-9}$ i.e. -45 dB, we infer an “instantaneous” conversion efficiency $P_{\text{idler}}(L) / P_{\text{probe}}(L)$ of -7 dB. The second method consists of calculating the ratio between the idler peak power (after subtracting the pump background) and the pump peak power from the output spectrum; this ratio, here equal to ~ 40 dB, is relevant due to the similar (pulsed) nature of both signals. By multiplying this ratio by the average output power measured when launching the pump only ($\sim 3 \cdot 10^{-6}$ W) and dividing it by the average output power associated with the probe transmission ($\sim 49 \cdot 10^{-6}$ W), we estimate the average conversion efficiency to be

around -52dB , leading us, again to an estimation of the instantaneous conversion efficiency $P_{\text{idler}}(L)/P_{\text{probe}}(L)$ of -7dB .

Although most reports about FWM in silicon nanowires refer to the conversion efficiency as $P_{\text{idler}}(L)/P_{\text{probe}}(L)$, the conversion efficiency given by Eq. (1), i.e. $P_{\text{idler}}(L)/P_{\text{probe}}(0)$, should be calculated with respect to the probe power at the entrance of the waveguide to avoid spuriously increasing the efficiency from having a very lossy waveguide [31]. From the estimation of the cw coupled probe power ($<0.4\text{mW}$), we can infer, using the ratio calculated above, $P_{\text{idler}}(L)/P_{\text{probe}}(0)$ to be $\sim -9.5\text{dB}$, which is reduced with respect to $P_{\text{idler}}(L)/P_{\text{probe}}(L)$ by the propagation loss of the probe across the chip.

The inset of Fig. 2(a) shows the associated idler peak power dependence on the probe power: it is linear, as expected from Eq. (1), with the slope corresponding to the -9.5dB conversion efficiency ($P_{\text{probe}}(0)$ taken as the reference). This linear variation measured at 1W pump power shows that nonlinear loss and free carriers due to the cw probe are negligible.

The result of the FWM simulations with the same input probe and pump parameters is displayed on Fig. 2(b). While Eq. (1) gives an insight into the FWM process, it does not take into account the effects of nonlinear losses and free carriers in silicon. From the numerical results, we can directly extract the conversion efficiency through taking the ratio of the idler peak power in the time domain and the cw probe respectively at the end and at the entrance of the waveguide. This gives an estimation of the instantaneous conversion efficiency $P_{\text{idler}}(L)/P_{\text{probe}}(0)$ of around -10dB that is constant for the probe power range investigated. This agrees well with the linear trend and the associated slope measured [see the inset of Fig. 2(a)].

3.2 Pump power dependence of FWM

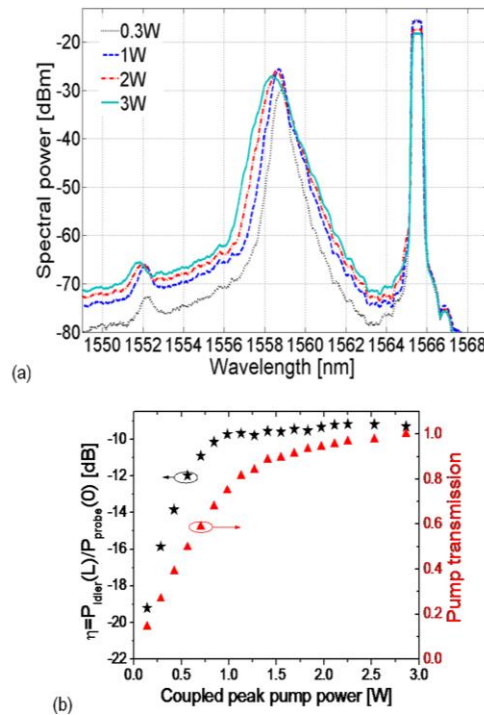


Fig. 3. (a) FWM spectra measured from the slow light PhC waveguide for $400\mu\text{W}$ cw probe at 1565.5nm , and increasing pump powers between 0.3W and 3W at 1559nm . (b) (black stars) Conversion efficiency $P_{\text{idler}}(L)/P_{\text{probe}}(0)$ extracted from (a) and (red triangles) normalized pump transmission as a function of pump power.

We next investigate the dependence of FWM on the pump power, at a constant probe power of $400\mu\text{W}$. Figure 3(a) shows the associated spectra with increasing pump power

between 0.3W and 3W. We observe a spectral broadening and blue shift of the pump due to self-phase modulation and free carrier dispersion [5], as well as a corresponding blue shift and spectral broadening of the idler peak, reemphasizing the strong correlation between the converted idler and pump signals. Figure 3(b) shows the instantaneous conversion efficiency $P_{\text{idler}}(L)/P_{\text{probe}}(0)$ as a function of the pump power, which increases until it saturates above $\sim 1\text{W}$ peak pump power. The saturation in the efficiency is caused by the slow light enhanced nonlinear losses, as attested by the strong roll-off of the pump signal transmission (red triangles) on Fig. 3(b). We measure a maximum instantaneous conversion efficiency $P_{\text{idler}}(L)/P_{\text{probe}}(0)$ of -9dB .

3.3 Comparison with the standard nanowire

We compare the measurements of the slow light PhC waveguide with that obtained from the nanowire with a ten times higher group velocity. Figure 4(a) shows the spectra measured from the nanowire, with a pump power equal to 1W and 3W, combined with a cw probe power of $25\mu\text{W}$ and $400\mu\text{W}$. While no idler signal is observed for the same input conditions as in Fig. 2(a) (dashed green line), a very weak idler signal above the ASE background is noticeable for 3W pump power and $400\mu\text{W}$ probe power. Note that in contrast to the slow light PhC waveguide, no SPM or free carrier induced blue shift is observed for the pump in the case of the nanowire, which is consistent with the slow light enhancement of these nonlinear effects [5]. Figure 4(b) displays the conversion efficiency $P_{\text{idler}}(L)/P_{\text{probe}}(0)$ inferred from these measurements when increasing the pump power (at a constant $400\mu\text{W}$ probe power). The conversion efficiency increases above the ASE background from about 1.2W pump power. Unlike the slow light PhC waveguide, no saturation of the conversion efficiency or of the pump transmission [red triangles on Fig. 4(b)] is observed towards higher pump powers. The maximum conversion efficiency, measured at 3W peak pump power, is $\sim -15\text{dB}$ ($P_{\text{probe}}(0)$ as a reference) and $\sim -14\text{dB}$ ($P_{\text{probe}}(L)$ as a reference), i.e. $\sim 6\text{-}7\text{dB}$ less than for the slow light PhC waveguide despite a three times larger pump power.

These FWM efficiencies should be compared with the difference in terms of $(\gamma P_{\text{pump}}L)^2$ between the two waveguides, as the FWM efficiency is to first approximation proportional to this product when leaving the loss and the phase mismatch ϕ aside [see Eq. (1)]. The $(\gamma P_{\text{pump}}L)^2$ factor for the slow light PhC waveguide is $[(2900 \times 80 \cdot 10^{-6}) / (170 \times 3 \times 80 \cdot 10^{-6})]^2$, i.e. 32 times larger than that for the nanowire: this should result in a $\sim 15\text{dB}$ difference, which is more than the 6dB measured. There are two reasons for this discrepancy. First, while the contribution due to the long, wide access ridges to FWM is negligible for the slow light PhC waveguide, this is not correct for the nanowire, providing an increase in the FWM efficiency in the latter case. When neglecting the tapered sections, the $(\gamma P_{\text{pump}}L)^2$ factor for the wide access waveguides is $\sim (30 \times 3 \times 800 \cdot 10^{-6})^2$ that is $\sim 6\text{dB}$ higher than for the short nanowire. The access waveguide contribution to FWM therefore dominates in the nanowire case, reducing the difference in the conversion efficiency with respect to that of the PhC waveguide down to $\sim 9\text{dB}$, which is closer to the 6dB experimental value. There may be also a residual contribution from the input patch cord since the associated $(\gamma P_{\text{pump}}L)^2$ factor ($\sim 0.5\%$) is comparable to that of the access waveguides. Secondly, the increased linear and nonlinear losses in the slow light PhC waveguide tend to degrade the conversion efficiency. The loss difference is reflected by the lower variation between $P_{\text{idler}}(L)/P_{\text{probe}}(L)$ and $P_{\text{idler}}(L)/P_{\text{probe}}(0)$ for the nanowire ($\sim 1\text{dB}$) as compared with the PhC waveguide ($\sim 2.5\text{dB}$).

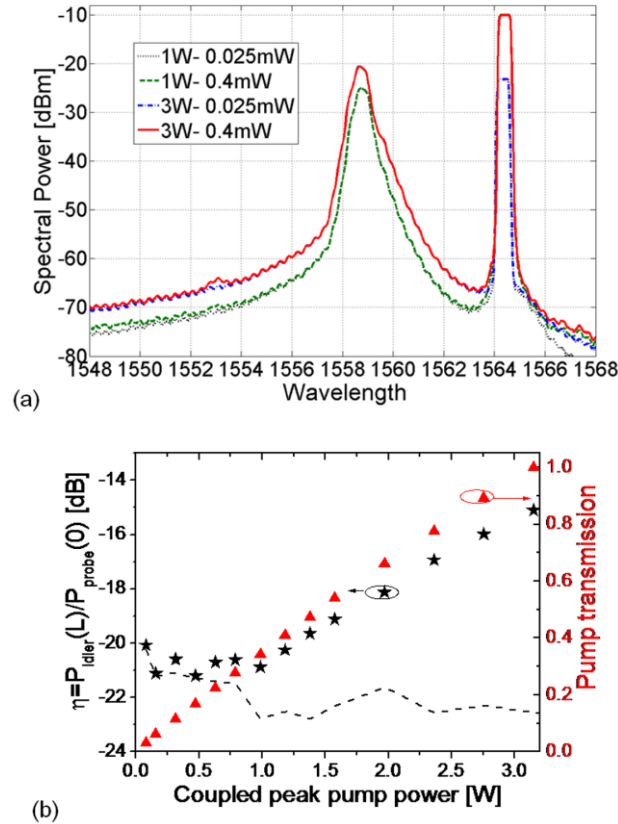


Fig. 4. (a) Spectra measured from the nanowire for 1W and 3W pump power (1559nm) and 25 μ W and 400 μ W cw probe power (1564.4nm) as indicated in the legend ($P_{\text{pump}}-P_{\text{probe}}$). (b) Conversion efficiency extracted from the data (black stars) at 400 μ W probe power and normalized pump transmission (red triangles) versus pump power. The dashed line is the minimum conversion efficiency that could be measured from (a) due to the ASE background.

3.4 Wavelength dependence of FWM

The main advantage of the dispersion engineered slow light PhC waveguide is the promise for maintaining a high conversion efficiency over a larger bandwidth than what is achievable with dispersive W1 PhC waveguides [26,29]. Due to the absence of anti-reflective coating at the end facets, though, we observed Fabry-Perot reflections that strongly modified the transmission (hence the coupling efficiency) of the probe when tuning the probe wavelength. It was therefore difficult to measure the FWM 3dB bandwidth with high accuracy. Figure 5(b) shows the instantaneous conversion efficiency $P_{\text{idler}}(L)/P_{\text{probe}}(0)$ extracted from the spectra in Fig. 5(a) obtained when tuning the probe wavelength between 1560.5 and 1567nm while keeping the pump in the middle of the flat band window (1559nm). The pump and probe powers are comparable to that of Fig. 2(a) and the probe coupling is assumed to be constant on Fig. 5(b). Despite the large variations due to the wavelength sensitive Fabry-Perot reflections of the cw probe, we can still observe that a relatively high conversion efficiency η of around $-14\text{dB} \pm 4\text{dB}$ is maintained up to 7nm pump-probe detuning.

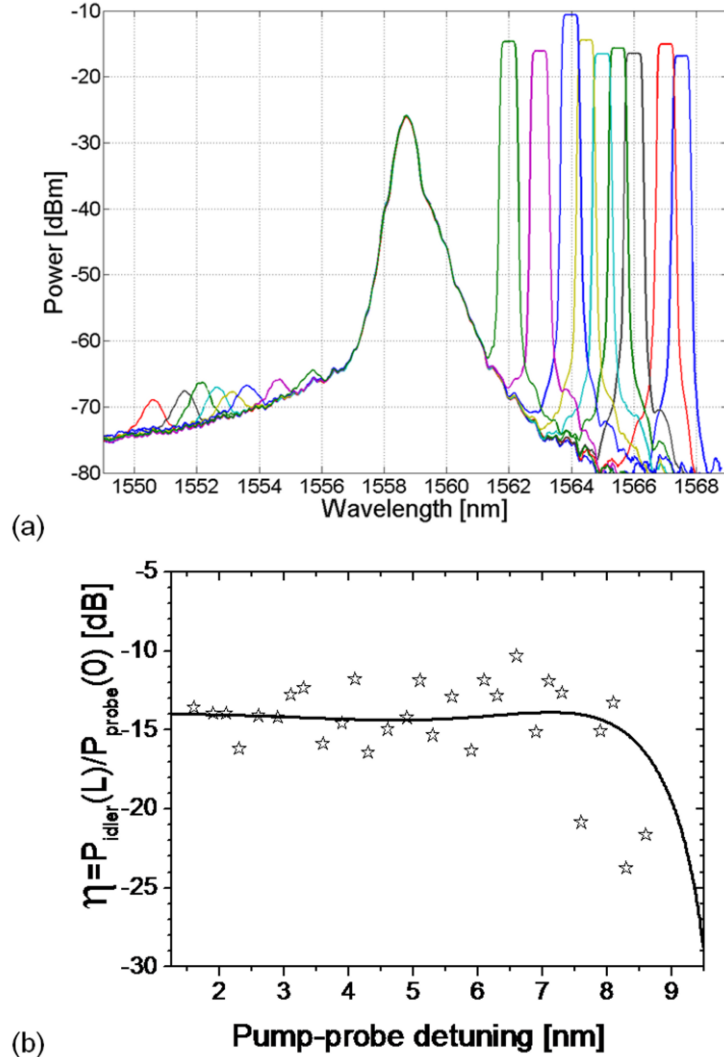


Fig. 5. (a) FWM spectra of the slow light PhC waveguide for different probe wavelengths when launching a constant coupled probe power of $400\mu\text{W}$, and a coupled peak pump power of 1W . (b) Associated FWM conversion efficiency (black stars) $P_{\text{idler}}(L)/P_{\text{probe}}(0)$ versus pump-probe detuning and (solid line) η calculated from Eq. (1).

4. Discussion

Although the parasitic Fabry-Perot reflections prevented us from measuring the FWM bandwidth with high accuracy, a relatively high efficiency is achieved for a pump-probe detuning up to 7nm . This gives a lower bound for the probe-idler conversion bandwidth of 14nm , which is roughly equal to the width of the engineered flat band slow light window, as theoretically expected [26]. Although this is much less than the bandwidth ($>100\text{nm}$) reported in dispersion engineered chalcogenide rib waveguides [24] and silicon nanowires [25,32] it is much larger than the values reported in dispersive W1 PhC waveguides at the band-edge [27,29], which are typically less than 1nm for $v_g = c/40$ [29] and 2nm for $v_g = c/10$ [27]. Here, the bandwidth is sufficient to use enhanced FWM afforded by these short slow light structures for specific applications such as signal regeneration of ultrafast optical signals [32].

The two main contributions to the FWM conversion efficiency $\eta = P_{\text{idler}}(L)/P_{\text{probe}}(0)$ in Eq. (1) –the nonlinearity $(\gamma P_{\text{pump}}L)^2$ and the dispersion induced phase mismatch ϕ – are compared in Table 1, at 1W pump power and 6nm pump-probe detuning, for the nanowire and the dispersion engineered PhC waveguide. As mentioned in section 3.3, the slow light enhanced nonlinear coefficient γ of the PhC waveguide leads to a $200 \times$ larger $(\gamma P_{\text{pump}}L)^2$ product than for the nanowire. This is less than a factor S^4 (~ 3000) difference due to the three-fold reduction in the effective area of the nanowire with respect to the PhC waveguide. When including the phase mismatch factor ϕ , the conversion efficiency of the slow light PhC waveguide is reduced by only $\sim 5\%$, providing a 20dB larger conversion efficiency than the nanowire of similar length. In most reports of FWM in silicon nanowires, the conversion efficiency is of the same order of magnitude, i.e. ~ 10 dB [25,32–35] or slightly larger [22,36,37] than the -9 dB reported here for the slow light PhC waveguide; but this is achieved in much longer nanowires –typically several millimeters [22] to a few centimeters [25,32–37]– and with several 100’s milliwatts pump power (except for 11W in [22]). The resulting $P_{\text{pump}} \times L$ product used in silicon nanowires lies between 1.8×10^{-3} [35,32] and 6.5×10^{-2} [22], i.e. roughly two orders of magnitude larger than the $P_{\text{pump}} \times L = 8 \times 10^{-5}$ product used in the slow light PhC waveguide. This shows the practical benefit of dispersion engineered slow light PhC waveguides in terms of reducing the device length without compromising the power consumption.

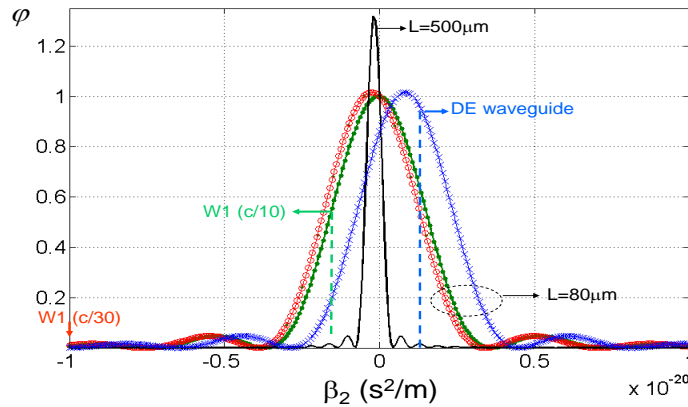


Fig. 6. Phase factor ϕ versus β_2 calculated for 6nm pump-probe detuning, 1W pump power and waveguides of length $L = 80\mu\text{m}$ (except for the black curve, $L = 500\mu\text{m}$). The red, green, and blue curves correspond to the three PhC waveguides with characteristics summarized in Table 1. Note that the blue curve ($\beta_4 = -6.10^{-46}$) is shifted towards larger β_2 values with respect to the green and red ($\beta_4 = 0$) curves, and the red curve is shifted towards lower β_2 values with respect to the green due to its higher γ .

Our -9.5 dB $P_{\text{idler}}(L)/P_{\text{probe}}(0)$ conversion efficiency compares favorably with the -36 dB [29] and -35 dB maximum conversion efficiency [27] measured in $440\mu\text{m}$ [29] and 1.3mm long W1 PhC waveguides [27] using band-edge slow light and $\sim 25\text{mW}$ cw pump power. In [27], this was achieved in a GaInP W1 waveguide with $c/10$ group velocity and similar γ ($\sim 2900/\text{W/m}$). Considering the 40 times lower power and the 16 times longer waveguide in [27], we estimate that the difference in the conversion efficiency expected from the ratio of $(\gamma P_{\text{pump}}L)^2$ for the two PhC waveguides should be ~ 8 dB in favor of the dispersion engineered waveguide, which is much less than the measured difference (>20 dB). First, the accumulated loss across the 1.3mm long waveguide in [27] adds an ~ 8 dB penalty to the overall conversion efficiency, as opposed to the short length used here. Recent results also suggest that the losses of engineered PhC waveguides are typically lower than W1s at equivalent group velocities [19]. Second, the 1.3mm length increases the detrimental impact of high dispersion, even for low detunings, due to the larger accumulated phase mismatch ($\phi \ll 1$). This is illustrated in Fig. 6, when comparing the black and red curve that shows the much faster ϕ variation with

dispersion for a 500 μm long waveguide compared with an 80 μm waveguide. Shortening the device is therefore critical when the dispersion of PhC waveguides is not engineered.

Table 1. Summary of the conversion efficiency predicted by Eq. (1) for 1W pump power for the two waveguides probed in section 3, compared with typical W1 PhC waveguides having either low v_g ($c/30$) and high (negative) dispersion or higher v_g ($c/10$) and lower dispersion. The conversion efficiency $\eta = P_{\text{idler}}(L)/P_{\text{probe}}(0)$ and the phase factor ϕ resulting from dispersion are calculated for 6nm pump-probe detuning. The waveguide length L , the propagation loss αL and second- and fourth-order dispersion β_2 and β_4 are indicated for the different structures

WG L [μm] αL [dB]	β_2 [s^2/m] β_4 [s^4/m]	γ [m^2/W]	$(\gamma \overline{P_{\text{pump}} L})^2$	Δk_L $\Delta\lambda = 6\text{nm}$	g^2 $\Delta\lambda = 6\text{nm}$	ϕ $\Delta\lambda = 6\text{nm}$	η $\Delta\lambda = 6\text{nm}$
Nanowire 80 μm 0.2dB	-4×10^{-25} negligible	170	1.8×10^{-4}	-8.6	1440	1	1.8×10^{-4} (-37dB)
DE PhC 80 μm ($n_g = 30$) 1.4dB	1.3×10^{-21} -6×10^{-46}	2930	0.047	5700	-2.3×10^7	0.95	0.038 (-14dB)
PhC W1 80 μm ($n_g = 30$) 1.4dB	-1×10^{-20} 0	2930	0.047	-2.2×10^5	-1×10^{10}	0.011	4.3×10^{-4} (-34dB)
PhC W1 80 μm ($n_g = 10$) 1.4dB	-1×10^{-21} 0	330	6.5×10^{-4}	-3.2×10^4	-2.5×10^8	0.57	3.5×10^{-4} (-35dB)

The expected FWM performance of W1 and dispersion engineered PhC waveguides of similar length (80 μm) are compared in Table 1, which includes two typical cases for the W1 waveguide: (i) low v_g ($c/30$) with high dispersion –consistent with measurements [29]– and (ii) moderate v_g ($c/10$) with lower dispersion. On the one hand, a standard W1 with the same v_g as the dispersion engineered PhC waveguide exhibits a conversion efficiency that is reduced through the ϕ factor by almost two orders of magnitude for only 6nm detuning, as represented by the blue and red arrows on Fig. 6. On the other hand, the reduced dispersion associated with a faster W1 mode ($v_g = c/10$) leads to a larger ϕ factor, as represented by the green arrow on Fig. 6, but the conversion efficiency is still two orders of magnitude less than for the dispersion engineered waveguide, because η varies as $\sim S^4$. Eckhouse *et al.* actually reached the same conclusion in [27]: the higher dispersion associated with a $c/10$ W1 PhC mode hindered the slow light enhanced γ coefficient to translate into higher conversion efficiencies than what was achieved with a $c/5$ faster mode. Engineering the dispersion of slow light PhC waveguides is therefore critical to exploit slow light enhanced γ factors and effectively increase the conversion efficiency of FWM processes, even for relatively small pump-probe detunings and short waveguide lengths. From Fig. 6, a three-fold reduction in the dispersion is enough to avoid compromising FWM in 80 μm long waveguides. Note that in silicon nanowires, phase matching becomes relevant only for long (\sim several mm) devices or large pump-probe detuning, due to their much lower dispersion.

The $\Delta k_L < 0$ dispersion in the W1 case may appear to be favorable to the conversion efficiency for high pump power, as g^2 can be made positive in that case (and $\phi > 1$) as soon as the pump power is high enough to satisfy $2\gamma \overline{P_{\text{pump}}} > |\Delta k_L|$. While this implies that negative dispersion should *a priori* be preferred whenever phase matched processes such as FWM are sought, increasing the overall conversion efficiency with the pump power is limited in silicon by nonlinear loss, as evidenced in section 3.2. Still, this suggests that the dispersion engineered waveguide used here, for which $\Delta k_L > 0$, may not provide the optimum FWM efficiency. Because of the short waveguide length and the limited pump power allowable in

silicon, the benefit afforded by the maximum phase factor ϕ in the 80 μm long slow light PhC waveguide is limited to $\sim 1\%$ –estimated through $\phi_{\text{max}} = [\sinh(g_{\text{max}}L)/(g_{\text{max}}L)]^2 \sim 1.016$ at 1W pump power. This is only about 7% larger than the phase factor ϕ estimated in the dispersion engineered PhC waveguide, as illustrated by the slight detuning of our waveguide dispersion indicated by the blue arrow from the maximum of the blue curve in Fig. 6. It is remarkable that while ϕ can be decreased significantly due to the typically high dispersion of slow light modes in PhC waveguides, its maximum value is bounded to ~ 1 in such short waveguides. In conclusion, the FWM conversion efficiency in short PhC devices ($< 100\mu\text{m}$) cannot be much improved over the $(\gamma P_{\text{pump}}L)^2$ factor through optimizing the phase matching, but it can be substantially degraded if one does not engineer the dispersion, as in W1 waveguides. Note that this conclusion is not so strong for PhC waveguides made of materials with lower nonlinear loss, such as chalcogenide glasses [28,38] and GaInP [27,39]. Because $g_{\text{max}} = \sqrt{\gamma P_{\text{pump}}}$, the improvement due to optimized phase matching (i.e. ϕ_{max}) can become more substantial when launching higher pump power in these waveguides.

6. Conclusion

In conclusion, we have experimentally investigated FWM in short (80 μm) dispersion engineered silicon PhC waveguides with a $(c/30)$ low group velocity, and measured an instantaneous conversion efficiency between the idler and the cw probe of $\sim -7\text{dB}$ (reference $P_{\text{probe}}(L)$) and $\sim -9.5\text{dB}$ (reference $P_{\text{probe}}(0)$) for 1W pump power. The comparison with a silicon nanowire shows that an increase of the conversion efficiency above a factor 10 is afforded by the slow light PhC waveguide but this figure is reduced by the contribution from the access waveguides. Engineering the PhC waveguide dispersion provides a probe-idler bandwidth of the FWM efficiency of at least 14nm, which is limited by the bandwidth of the slow light window. The dispersion engineered PhC waveguide therefore allows us to exploit the slow light enhanced nonlinearity for increasing the conversion efficiency, without significantly compromising the bandwidth, in contrast with previous reports of FWM based on dispersive slow light in relatively longer W1 waveguides. Engineering the dispersion of slow light PhC waveguides is critical, even for short devices ($< 100\mu\text{m}$) because of the typically high dispersion associated with slow light modes in these structures. In addition, the FWM performance of the dispersion engineered PhC waveguide compares well with that of silicon nanowires, when length and input power in the different experiments are accounted for. These results suggest that optimized slow light PhC waveguides could have interesting applications for realizing ultra-short nonlinear functions for all-optical signal processing.

Acknowledgement

The authors acknowledge Mike Lamont for helpful discussions. The support of the Australian Research Council through its Centre of Excellence and Discovery grant programs is gratefully acknowledged as well as the EU-FP7 Marie Curie Fellowship project “OSIRIS”. Additional acknowledgment is given to the support of the International Science Linkages Program of the Department of Education, Science and Technology. The silicon samples were fabricated in the framework of the EU-FP6 funded ePIXnet Nanostructuring Platform for Photonic Integration (www.nanophotonics.eu).